Journal of Pharmaceutical Sciences 114 (2025) 394–401

Contents lists available at ScienceDirect

Journal of Pharmaceutical Sciences

journal homepage: www.jpharmsci.org

Research Article

Mechanisms of drug release from a melt-milled, poorly soluble drug substance

Dominik Sleziona[a], David R. Ely[b], Markus Thommes[a,*]

[a] TU Dortmund, Department of Biochemical and Chemical Engineering, Laboratory of Solids Process Engineering, Emil-Figge-Str. 68, 44227 Dortmund, Germany
[b] Ivy Tech Community College, 3101 S Creasy Ln, Lafayette, IN 47905, USA

ARTICLE INFO

Article history:
Received 7 July 2024
Revised 10 October 2024
Accepted 10 October 2024
Available online 18 October 2024

Keywords:
Drug release
Melt milling
Paddle apparatus
Solid crystalline suspension
Phase-field simulation
Surface reaction

ABSTRACT

Increasing the dissolution kinetics of low aqueous soluble drugs is one of the main priorities in drug formulation. New strategies must be developed, which should consider the two main dissolution mechanisms: surface reaction and diffusion.

One promising tool is the so-called solid crystal suspension, a solid dispersion consisting of purely crystalline substances. In this concept, reducing the drug particle size and embedding the particles in a hydrophilic excipient increases the dissolution kinetics. Therefore, a solid crystal suspension containing submicron drug particles was produced via a modified stirred media milling process. A geometrical phase-field approach was used to model the dissolution behavior of the drug particles.

A carrier material, xylitol, and the model drug substance, griseofulvin, were ground in a pearl mill. The in-vitro dissolution profile of the product was modeled to gain a deep physical understanding of the dissolution process. The used numerical tool has the potential to be a valuable approach for predicting the dissolution behavior of newly developed formulation strategies.

Introduction

Many newly developed drug substances suffer from low aqueous solubility, but their advantages have forced the pharmaceutical industry to develop new formulation concepts to overcome the solubility issues.[1] Therefore, classification of those substances based on their solubility and permeability was proposed by Amidon et al.[2] Currently, the influence of starting material characteristics like powder flowability and particle size and shape on formulation strategies for oral administration is discussed.[3]

Several extension models based on Fick's law[4] of diffusion have been derived to describe the dissolution behavior of drug substances. In addition to the dissolution from a flat surface[5] or a spherical particle,[6] the diffusion of an API from an ointment into the skin has been also described mathematically.[7] A comparatively new approach accounts for surface reaction effects in drug substance dissolution behavior.[8,9] In the literature, phase-field simulations have been used as a numerical tool to model the mass transfer behavior of substances capturing both surface reaction and diffusion kinetics.[10–12]

In addition to changing the crystal habit, poly- or pseudopolymorphs, complex compounds and surfactants, a promising tool to increase the solubility as well as the dissolution rate of APIs in water is solid dispersions.[13,14] The dispersion of crystalline drug particles in a crystalline matrix is called a solid crystal suspension (SCS), and symmetric sugar-alcohol molecules have been identified as particularly effective carriers.[15] This crystalline mixture, in which no molecular interaction between drug and excipient takes place, exhibits inherent storage stability and has enabled a further field of application in solid dosage formulation. According to the Nernst-Brunner law,[16,17] a decrease in particle size increases the dissolution rate of a substance. In solid crystal suspensions, this effect is enhanced by improved wettability[18] caused by the dissolving excipient. While already published production processes like cogrinding[19] and hot melt extrusion[20] are indeed robust processes, comminution of the crystalline API particles into the submicron region is only conditionally possible.

One advantage of submicron particles is a further increase of the dissolution rate due to the ratio between surface tension and curvature of particles according to Ostwald-Freundlich.[21,22] Often used top-down manufacturing methods in pharmaceutical literature are

* Corresponding author at: TU Dortmund, Department of Biochemical and Chemical Engineering, Laboratory of Solids Process Engineering, Emil-Figge-Str. 68, 44227 Dortmund, Germany.
E-mail address: professors.fsv.bci@tu-dortmund.de (M. Thommes).

https://doi.org/10.1016/j.xphs.2024.10.016

high-pressure homogenization[23,24] and stirred media milling for submicron particle production.[25,26] The aim of this work was to use a geometrical phase-field approach[27] to model the dissolution behavior of a solid crystal suspension containing submicron drug particles. Therefore, the established process of stirred media milling was modified to grind API particles directly in a sugar alcohol melt down to the submicron region (see Fig. 1).

The results of the subsequently performed dissolution experiments with the melt-milled SCS were modelled with a phase-field simulation in order to elucidate the drug-release mechanisms.

Materials and methods

Materials

In this study, micronized griseofulvin (Hawkins, Roseville, USA) with a median particle diameter of 15 μm was used as a model drug substance, and the sugar alcohol, xylitol (Xylisorb, Roquette, Lestem, France), was used as the carrier excipient due to its low melting temperature ~92 °C, and its hydrophilic properties. Deionized water served as the solvent in all dissolution experiments, and sodium dodecyl sulfate was used as an additive in the particle size measurements to prevent agglomeration.

Meltmilling

A pearl mill (Rheosyst 1000, Coesfeld, Germany) was used to set up the melt-milling experiments with a specific energy of 1.5 MJ·kg^{-1}. The glass milling chamber was heated in an oil bath up to 120 °C. 1 mm zirconia beads (Fritsch, Idar-Oberstein, Germany) were used as grinding media where the milling chamber was filled up to 90 % of its capacity. A physical mixture of xylitol and 10 % (w/w) griseofulvin was heated up to 120 °C to melt the xylitol. The griseofulvin remained crystalline and was suspended in the xylitol melt. This system was treated in the pearl mill for 8 hr at 800 rpm. A 500 μm sieve was used to extract the grinding media from the produced SCS.

Particle size measurements

The sphere-equivalent particle sizes were determined using a laser diffraction particle size analyzer (Mastersizer 3000, Malvern Panalytical, Malvern, United Kingdom). A dispersion agent of 1 % (w/w) sodium dodecyl sulfate was added to the sample, which afterwards was dispersed using a wet-sample dispersion unit (Hydro EV, Malvern Panalytical, Malvern, United Kingdom) in a saturated, filtered griseofulvin-water solution to avoid agglomeration. (Fisherbrand, ThermoFischer Scientific, Waltham, USA) was used for filtration. The stirrer speed was set to 2000 rpm, the refractive index was 1.565, and the adsorption index was 0.01. Six replicate measurements ensured the reproducibility of the measured particle-size distributions. The measured particle-size distributions of the melt-milled powder were used in a MATLAB code (R2016b, The MathWorks, Natrick, USA) as source distributions to randomly generate digital samples. This sample was packed into a two-dimensional domain. The locations (x- and y-coordinates of the center points of the circular particles) as well as the diameters were saved in csv-file that could be implemented as the initialization list for the phase-field simulation.

Dissolution experiments in the paddle apparatus

The dissolution profile of the micronized griseofulvin, a physical mixture, an unmilled SCS, and the melt-milled SCS were analyzed in the USP apparatus II (DT6, Erweka, Langen Germany) with a paddle speed of 50 rpm. For all dissolution experiments, one liter of deionized water at 37 °C was used, and 2 mg of griseofulvin particles were submerged in the dissolution medium. Sink conditions were maintained. A UV/VIS spectrometer (Lambda 2, Perkin Elmer, Ueberlingen, Germany) was used to quantify the griseofulvin release, using 5 cm cuvettes and a wavelength of 294 nm.

Phase-field simulation

The geometrical phase field approach is a modelling technique where the concentration as well as phase transformations are considered with respect to space and time. This technique is widely used in material science[28–30] and was recently adopted for pharmaceutical applications. This enables the dissolution process to be modeled while accounting for different shapes and anisotropy,[31] which cannot be readily done with other techniques. Similar to previous work,[32] the geometrical phase-field approach according to Beckermann et al.[27] was used to simulate the two dimensional dissolution behavior of the melt-milled SCS. In this approach, a non-conserved order parameter, Φ, is used to describe the long-range molecular order of

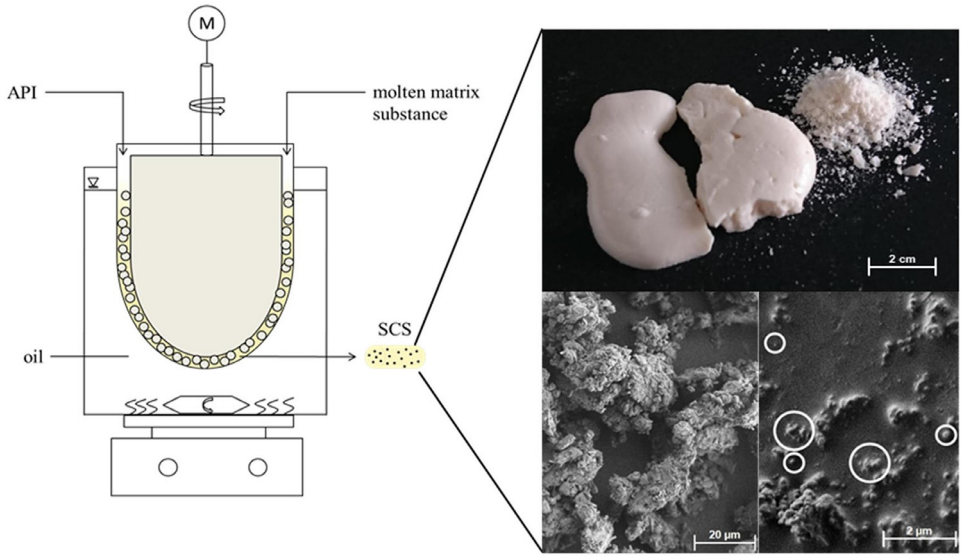

Fig. 1. Schematic drawing of the melt-milled process (left), macroscopic image (top right) and SEM image (bottom right).

the system. The value of the parameter varies from 0 to 1, where 0 corresponds to a perfectly disordered system (e.g., liquid melt) and 1 corresponds to a perfectly ordered system (e.g., crystalline solid). The phase in space and time evolves according to

$$\frac{\partial \Phi}{\partial t} = \mu_k \Gamma \overbrace{\left(-\nabla^2 \Phi + \frac{\Phi(1-\Phi)(1-2\Phi)}{\delta_{SR}^2}\right)}^{\text{interfacial tension term}} + \mu_k \overbrace{\left(T_m - T - m_l \frac{w}{1-\Phi+k\Phi}\right)}^{\text{thermal driving term}} \frac{\Phi(1-\Phi)}{\delta_{SR}} \tag{1}$$

Here, the phase change over space and time is expressed by the interface mobility μ_k, the interfacial tension term, and a thermal driving term, where Γ is the Gibbs-Thomson coefficient, δ_{SR} is the interface thickness, T_m is the melting point of the pure substance, T is the temperature of the system, m_l is the slope of the liquidus line, k is binary partition coefficient, and w is weight fraction (concentration). While the interfacial tension term opposes the phase change, the thermal term favors it.

Since, during dissolution, the phase transition is always coupled with a diffusion process, this could be expressed by the general convection-diffusion equation. By adding the dimensionless Sherwood number (Sh_m - ratio of total mass transfer and diffusion) to the weight fraction gradient, an isotropic fluid flow in all directions could be approximated without knowing the fluid velocity vector field. The rate change of the concentration field, in terms of weight fraction w, with respect to time is thus expressed as follows:

$$\frac{\partial w}{\partial t} = \nabla \cdot \tilde{D}\left[(1+Sh_m)\nabla w + \frac{(1-k)w}{(1-\Phi)+k\Phi}\nabla\Phi\right] \tag{2}$$

Here $\tilde{D}$ is the phase averaged diffusivity, ∇w is the gradient of the weight fraction (concentration), and $\frac{(1-k)w}{(1-\Phi)+k\Phi}\nabla\Phi$ is a diffusive flux term. The diffusive flux term, which acts like a sink or source term directly related to the phase, enables the coupling of the phase and weight fraction equation.

Simulations conducted by solving these equations simultaneously were written in python 2.6.6 (Python Software Foundation, Wilmington, USA) using Fipy 3.0.1.[33] Results were visualized with Matplotlib. A Linear LU-Solver was used to simultaneously solve the partial differential equations. All simulations were run on a DELL PowerEdge R720 equipped with an Intel Xeon E-26XX processor with 32 cores, and 64 gigabyte-RAM. The total computational time took two weeks.

Surface tension measurements

A 0.018 % (w/w) xylitol-deionized water solution, corresponding to the xylitol concentration in the USP apparatus II, as a polar fluid and diiodomethane as a non-polar fluid were used to measure the static contact angle between these fluids and griseofulvin. Five biplane tablets with a diameter of 13 mm and a weight of 300 mg ± 10 mg were produced by a hydraulic press (Type 3, Paul Weber, Bösingen, Germany) with a force of 25 kN for about 30 s. A drop of the corresponding fluid was placed by the drop shape analyzer (G40, Krüss GmbH, Hamburg, Germany) on the surface, and the contact angle was measured automatically after one second by the Krüss analyzing software. A surface tension of 11 mJ·m^{-2} between griseofulvin and the xylitol solution was calculated based on the results of the contact angle measurements, Young's equation, and the model from Owens and Wendt.[34]

Scanning electron microscope

Micrographs from a scanning electron microscope (SEM) were made of micronized griseofulvin and the griseofulvin particles of the melt-milled solid crystal suspension (H-S4500 FEG, Hitachi High-Technologies Europe, Krefeld, Germany). To analyze the particle size of the griseofulvin particles embedded in the carrier excipient, the matrix was dissolved in a saturated and filtered griseofulvin-water solution. Afterwards, the sample was treated for 120 s with a disperser (ULTRA-TURRAX, T25, IKA Werke, Staufen im Breisgau, Germany) equipped with a dispersing tool (S 25 H-25 F, IKA Werke, Staufen im Breisgau, Germany) to reduce agglomerates.

Differential scanning calorimetry

According to the method of Mühlenfeld et al. ,[19] the melt-milled solid crystal suspension was compared to a griseofulvin sample with an amorphous content of 1 % (w/w) and pure xylitol. For this purpose, amorphous griseofulvin was prepared by quenching a griseofulvin melt. The amorphous state was subsequently confirmed in the DSC. Samples between 9 mg and 11 mg were weighed into 45 mg aluminum pans and afterwards heated in the differential scanning calorimeter (DSC Q2000, TA Instruments, New Castle, USA). Each specimen was measured three times with a heating rate of 10 K·min^{-1} over a temperature range of 0 °C to 250 °C.

Results and discussion

Characterization of the melt-milled product

To verify that the production of submicron particles via the melt-milling process is possible, particle size measurements were performed. In Fig. 2, the cumulative volume distribution is plotted as a function of the particle diameter. It could be observed that, compared to the micronized starting material, the distribution of the melt-milled solid crystal suspension was shifted into the submicron region (0.1–1 μm). The d_{90} showed that 90 % of the starting material had a particle size smaller than 32.3 μm while the griseofulvin particles of the produced solid crystalline suspension had a d_{90} of 0.96 ± 0.02 μm. This indicates that the melt-milling method was able to disperse and grind particles directly in a sugar-alcohol melt.

During the melt grinding process, the drug particles were dispersed in a xylitol melt of 120 °C and at the same time subjected to mechanical stress of the grinding media. In order to show that the crystallinity of the educts was retained, DSC measurements were performed to assess the solid states in the melt-milled product. A sample of the product from the melt-milling process (SCS) was compared to a mixture of 99 % (w/w) crystalline griseofulvin and 1 % (w/w) amorphous griseofulvin as well as to the pure carrier matrix material, xylitol. The results are shown in Fig. 3 where the heat flow is plotted against the temperature. Exothermic events are defined in positive y-axis direction. The characteristic endothermic melting peak of xylitol (92 °C–95 °C)[35] can be seen in the SCS sample and for pure xylitol. A

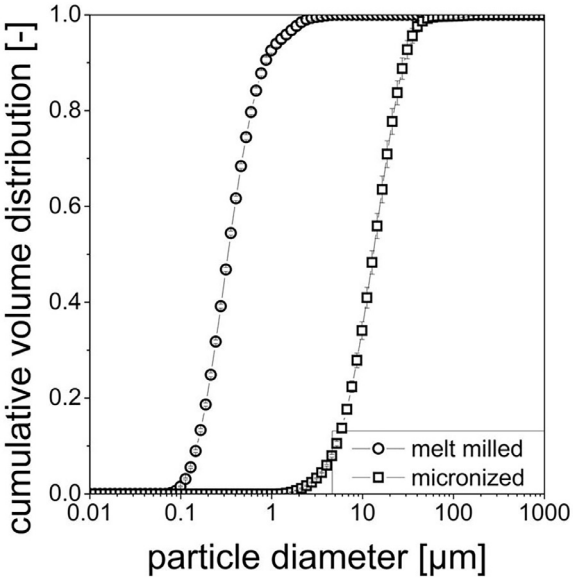

Fig. 2. Cumulative particle size distributions of micronized and the melt-milled drug (av ± sv, $n = 6$) measured by laser diffraction.

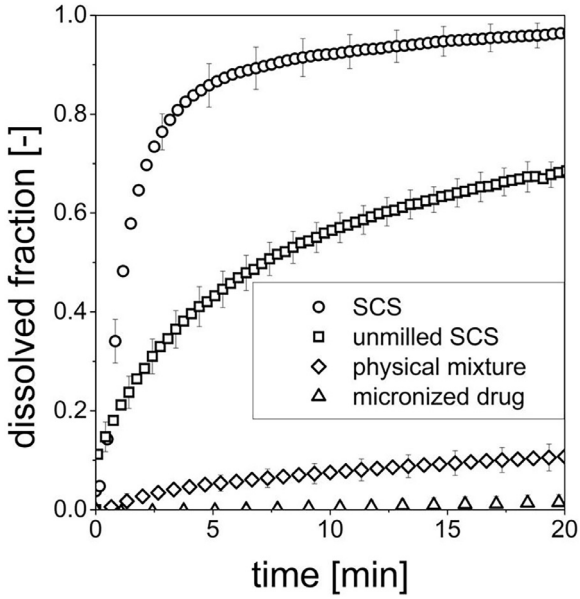

Fig. 4. Dissolved fraction of the melt-milled solid crystal suspension, an unmilled solid crystal suspension (micronized griseofulvin dispersed in a xylitol melt), a corresponding physical mixture, and pure micronized griseofulvin (av ± sv, $n = 3$).

corresponding characteristic melting peak for crystalline griseofulvin (~219 °C)[36,35] was detected for the mixture containing 1 % amorphous drug and the melt-milled SCS, respectively. In order to be able to make a quantitative statement about the amorphous proportion of griseofulvin in the melt-milled product, it should be examined whether an exothermic recrystallization peak can be observed after the glass transition temperature.[37] For the 1 % amorphous sample, the recrystallization peak was observed at ~140 °C in the enlarged portion of the DSC thermogram (Fig. 3, right side). Despite the long exposure to thermal and mechanical stress for the melt-milled SCS, no endothermic recrystallization peak of the drug could be observed, indicating that the system remained crystalline.

In vitro dissolution experiments were conducted in the USP apparatus II to analyze the dissolution behavior of the melt-milled solid crystal suspension, an unmilled solid crystal suspension (micronized griseofulvin dispersed for 120 s in a xylitol melt via Ultra-Turrax equipped as in section Scanning electron microscope), a corresponding physical mixture, and pure micronized griseofulvin. In Fig. 4, the dissolved fraction of these submerged samples is plotted as a function of the dissolution time, where 1.0 corresponds to 100 % of the contained drug. Since micronized griseofulvin has very poor wettability, it had the lowest dissolution rate.

An improvement is realized by embedding the micronized griseofulvin in xylitol. The highly hydrophilic excipient increased the dissolution rate by a factor of 10. Further particle size reduction into the submicron region, via melt milling, enabled an additional increase in the dissolution rate. Especially in the first two minutes, the melt-milled solid crystal suspension saw an overwhelming increase of the dissolution rate.

Phase-field simulation of the dissolving, melt-milled solid crystal suspension

In order to understand the mechanism of the investigated dissolution process of the submicron sized griseofulvin particles in the melt-milled solid crystal suspension, a phase-field simulation was

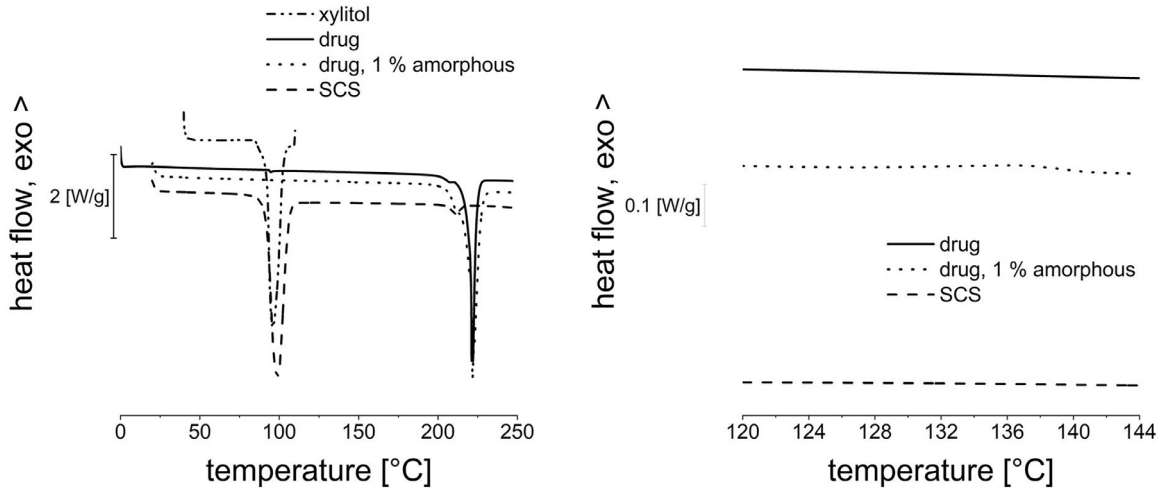

Fig. 3. DSC thermogram of pure griseofulvin, pure xylitol, griseofulvin with an amorphous content of 1 %, and the melt-milled SCS product (left). Enlarged region of DSC thermogram from 120 °C to 144 °C (right). Exothermic events were defined in positive y-axis direction.

created.[38–42] Therefore, the measured particle size was used to initialize simulated particles in a two-dimensional mesh. Based on previous works of the authors, where the model was compared to the corresponding analytical equations, it could be assumed that the carrier material, xylitol, dissolves instantaneously in relation to the drug substance.[32] A change in the surface tension between griseofulvin and the dissolution solvent was considered in the performed surface tension measurements (section Surface tension measurements). According to section Phase-field simulation, the temporally changing flow conditions with characteristic vortices[43–45] in the USP apparatus II vessel could be taken into account by calculating the median Sherwood number. Therefore, a median velocity v_m of 0.0485 m·s^{-1} was used, determined by laser doppler measurements of McCarthy et al. in the apparatus II at 50 rpm.[44] Together with the median of the measured particle size distribution of the melt-milled SCS, $d_{50,}$ the median particle Reynolds number (ratio of inertial and viscous forces) could be determined. For a single spherical particle, the Schmidt number (ratio of viscous diffusion and mass diffusion) and the median Reynolds number can be correlated to calculate the median Sherwood number.[46,47]

$$Sh_m = 0.991 \cdot (Re_m \cdot Sc)^{\frac{1}{3}} = 0.991 \cdot \left(\frac{d_{50} \cdot v_m \cdot \rho_{liquid}}{\eta} \cdot \frac{\eta}{\rho_{liquid} \cdot D} \right)^{\frac{1}{3}} \quad (3)$$

Here η is the dynamic viscosity, ρ_{liquid} is the density of the liquid, and D is the diffusivity of the drug substance in water.

Based on the measured particle size of the melt-milled product (Fig. 2), a digital sample of 150 circular, two-dimensional, isotropic griseofulvin particles were initialized. The square domain with a length and height of 3.4 μm was discretized into square cells with an edge length of 2 nm. The dissolution process in the 0.018 % (w/w) xylitol-water solution could be observed via the simultaneously evolving phase (Fig. 5 left, upper side) and concentration fields (Fig. 5 left, lower side). Table 1 shows the parameters and associated values used in the numerical simulation.

Since the entirety of the obtained visualizations could not be displayed, a selection is presented at defined time steps of the simulation. Around the red, solid, isotropic crystal ($\Phi = 1$) the phase transition appeared as light-colored ring at the solid-liquid interface and the mass transfer appeared as a black. The chosen Dirichlet boundary conditions[48] ensure sink conditions. Thereby, the dissolved griseofulvin could leave the system which led to a total dissolution of the particles.

Table 1
Experimental and calculated simulation parameters for griseofulvin and water (*griseofulvin in water, ** water in crystalline griseofulvin).

Parameter	griseofulvin	water
Melting temperature [K]	489	273
Melting enthalpy [J·g^{-1}]	96.04	256
Diffusion coefficient [m^2·s^{-1}]	$7.09 \times 10^{-10*}$	$7.09 \times 10^{-25**}$
System temperature [K]	310.15	
Surface tension solid/water [J·m^{-2}]	1.1×10^{-2}	
Interfacial thickness [m]	1.0×10^{-9} / 2.0×10^{-9}	
Slope of the liquidus line [K]	1.71×10^{6}	
Saturation concentration [%]	2.18×10^{-3}	
Interface velocity [m·s^{-1}]	5.25×10^{-10}	
Sherwood number [-]	2.93	

In the authors previous works, a two-dimensional, analytical equation was introduced, which described a cylinder dissolving under sink conditions over its lateral surface limited by the surface reaction in which the diameter of the cylinder evolved in time.[32]

$$d = d_0 - \frac{2 \cdot k_{SR} \cdot w_{solid}}{\delta_{SR}} \cdot t = d_0 - 2 \cdot v_n \cdot w_{solid} \cdot t \quad (4)$$

Here, the initial diameter of a particle, d_0, is reduced by the product of the interface velocity, v_n, the weight fraction of the solid, w_{solid}, and the dissolution time, t. Thereby the interface velocity could be expressed via the surface reaction coefficient, k_{SR}, and the interfacial thickness, δ_{SR}. Based on the Hixson-Crowell cube root law, Eq. (4) can be also adapted to account for a 3D spherical particle to calculate the remaining mass m_R.[49]

$$m_R^{\frac{1}{3}} = m_0^{\frac{1}{3}} - v_n \cdot w_{solid} \cdot \rho_{solid} \cdot \left(\frac{4 \cdot \pi}{3} \right)^{\frac{1}{3}} \cdot \left(\frac{1}{\rho_{solid}} \right)^{\frac{2}{3}} \cdot t \quad (5)$$

Here, initial mass of a particle, m_0, is reduced by the product of the interface velocity, v_n, the weight fraction, w_{solid}, the solid density, ρ_{solid}, and the dissolution time, t. The application of this equation on every single particle size fraction of the measured particle-size distribution of the melt-milled product (Fig. 2) provided a second prediction option for the dissolution process.

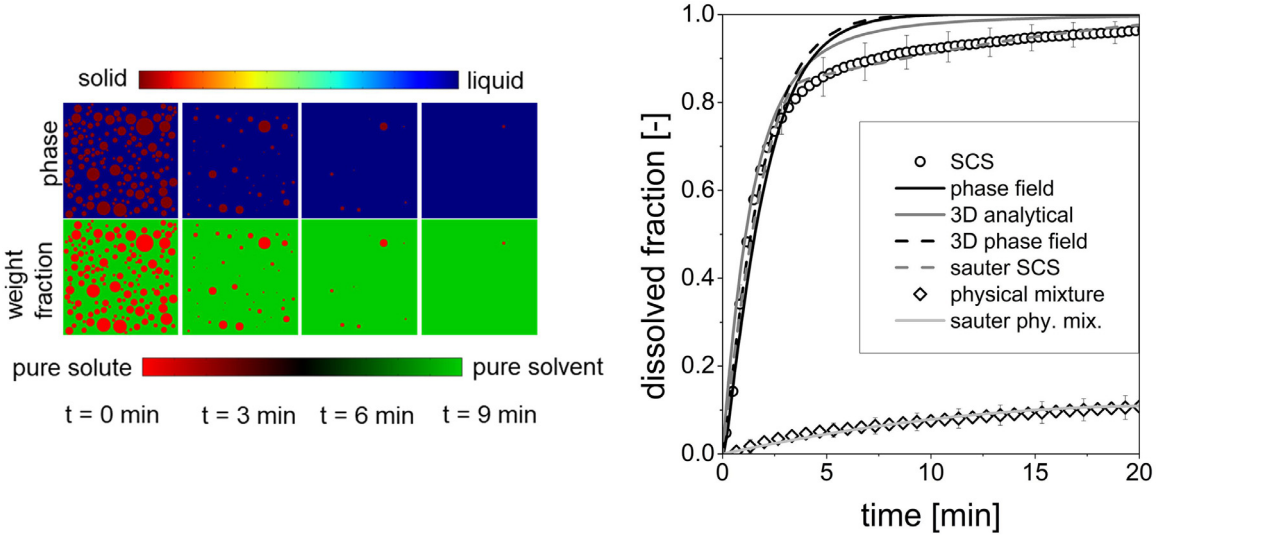

Fig. 5. Simulated dissolution process of 150 circular, two-dimensional, isotropic griseofulvin particles. The particle size is based on the measured, cumulative particle-size distribution (see Fig. 2). The Sherwood number was calculated based on the flow conditions in the USP apparatus II (left). Dissolved fraction of the melt-milled solid crystal suspension measured in the USP apparatus II, the phase-field simulation, adapted in 3D, the 2D/3D analytical equation, the 2D Sauter diameter for the melt-milled solid crystal suspension, and the physical mixture over dissolution time (right).

Since the results obtained were output in 2D by the phase-field simulation, the calculation had to be adjusted to account for the third dimension. The resulting dissolved fraction of the phase-field simulation as well as the analytical result for spherical particles could be plotted together with the results of the in vitro dissolution study as a function of the dissolution time in Fig. 5. The rapid increase of the dissolution profile in the first five minutes was accurately captured by the phase-field simulation as well as by the 3D analytical equation. Subsequently, a higher difference between the dissolved fraction of the melt-milled solid crystal suspension and both prediction tools could be observed.

This could be explained by the fact that both tools, the phase-field simulation and the analytical equation, model the dissolution kinetics of the melt-milled product as isotropic particles. Additionally, agglomeration of the drug particles during dissolution as well as the complex flow in the USP apparatus II vessel were not accounted for. Only the flow conditions were considered and were approximated by the Sherwood number.[50] Moreover, the domain space and the resulting number of griseofulvin particles was several orders of magnitude smaller compared to the experimental set up.

It turns out that the two-phase nature of the release cannot be explained or depicted by a shape parameter. The difference between the release experiment and the simulation can therefore be explained by agglomerate formation. With the aim of capturing this two-phase nature, the experimental data of the drug dissolution from the melt-milled SCS as well as the physical mixture were simulated using a "2D Sauter" diameter ($d_{2/1}$), introduced by Mugele and Evans as the so called surface diameter.[51]

$$d_{2/1} = \frac{surface\ area}{diameter} = \pi \cdot d \tag{6}$$

The results indicate that, in addition to primary agglomeration, the agglomerate shape and anisotropy of the particles may also influence the deviation between the experimental data and the phase-field simulation.

Sauter diameter

To evaluate if the influence of agglomerate shape on the release kinetics must also be taken into account, the dissolution of an arbitrarily formed agglomerate with an area of 1.46 μm^2 is compared to area equivalent particles in varying numbers. Fig. 6 illustrates the particle initialization, where the domain was meshed with square elements with an edge length of 1 nm.

The dissolution of one, two, three, five, and ten, circular-particle systems with equivalent area, one agglomerate with equivalent area, and one 2D Sauter diameter ($d_{2/1}$) particle were simulated. Their phases as well as concentration profiles after a dissolution time of 1.5 min are shown in Fig. 6 as an example. The entire release curves are shown in Fig. 7. As the number of particles increases, the surface-to-volume ratio increases and thus accelerates the release.

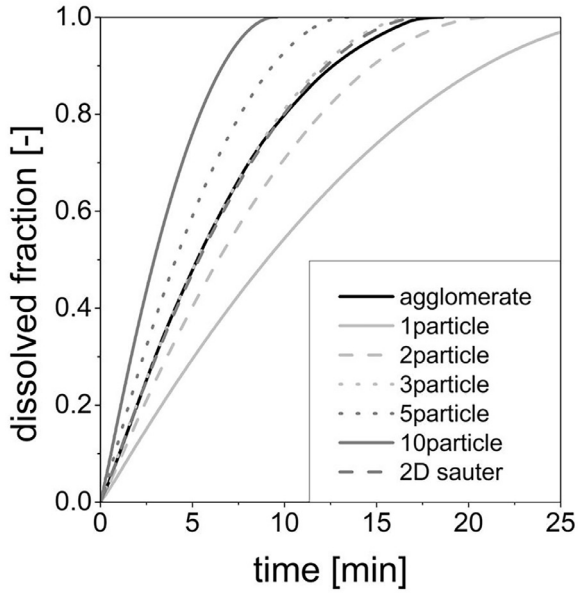

Fig. 7. Dissolved fraction of a griseofulvin agglomerate and an area equivalent number of particles as well as a circular particle with the 2D Sauter diameter corresponding to the agglomerate.

The release curve of the agglomerate was best represented by the three-particle system and the 2D Sauter diameter. This is due to an approximately equal surface to volume ratio. The results show that the dissolution of an arbitrarily shaped agglomerate can be approximated by the corresponding 2D Sauter diameter.

Anisotropy

In the simulations described above, the release behavior of isotropic particles was investigated. Since, according to Gibbs, the surfaces in a crystal always try to take up a minimum of free energy, the surface tension is directly proportional to the geometry of the surface.[52–54] It is also known that griseofulvin can form several polymorphs[55,56]; form I was used in the experimental investigations. In the following phase-field study, the dissolution behavior of griseofulvin polymorphs of form I and II was simulated to evaluate the effect on the dissolution process. The characteristic parameters were taken from the publication by Su, X., et al.[55] For the implementation of the anisotropic behavior, the common method of a surface tension tensor in the implicit diffusion term of the phase equation was used.[57,33]

$$\sigma' = \sigma \cdot \begin{pmatrix} x & 0 \\ 0 & y \end{pmatrix} \tag{7}$$

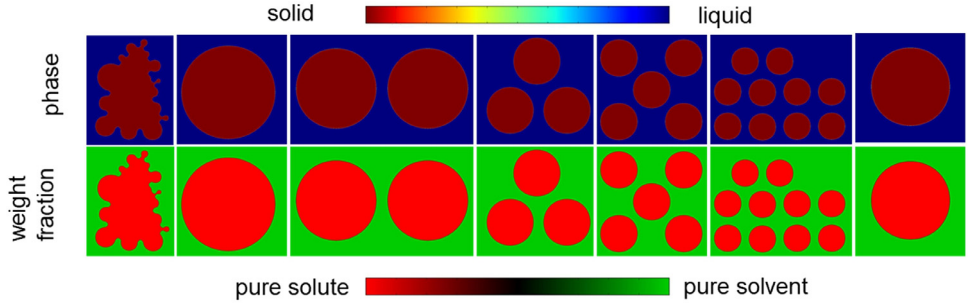

Fig. 6. Example pictures at a time point of 1.5 min of a two-dimensional, isotropic agglomerate of griseofulvin and the area equivalent number of isotropic, two-dimensional, circular particles as well as a circle with the corresponding 2D Sauter diameter.

Table 2
Anisotropy values used for the griseofulvin polymorphs form I and form II according to Su, et al. .[55]

Name	x-vlaue	y-value
Form I_aniso	1.0	4.277
Form I_iso	1.0	1.0
Form II_aniso_needle	1.0	4.277
Form II_aniso	1.0	1.18
Form II_iso	1.0	1.0

Two simulations were carried out for the acicular form I as anisotropic and isotropic crystals, and three for the rhombic form II as anisotropic, isotropic, and anisotropic needle crystals, which has hypothetical anisotropic properties like the acicular form I. The surface tensor values used can be found in Table 2.

Fig. 8 shows the different forms of the two polymorphs and the dissolved fraction over time. The data shows that the anisotropic properties of the crystal have no significant influence on the dissolution behavior for form II.

For the acicular form I, on the other hand, an influence of the pronounced anisotropy can be detected. However, if the same anisotropic behavior for form II as for form I is assumed, a greater influence on the dissolved fraction can be observed. This shows that strong anisotropy such as for the needle-shaped form I could have an effect on the dissolution behavior. However, slight anisotropy as seen for the rhombic form II cannot contribute to a two-phase dissolution process as seen for the melt-milled SCS.

Conclusion

To overcome the low aqueous solubility of drug substances, a new production method of preparing solid crystal suspensions containing submicron particles was discussed. The melt-milling concept offered the opportunity to grind drug particles below 1 μm and embed them directly in a sugar alcohol matrix within one formulation step. A high storage stability, based on the crystalline state of the product, and an increased dissolution rate of more than 30 % characterized the melt-milled product.

The in vitro dissolution results could be modeled by using a geometrical phase-field approach and an analytical equation. The trend of both tools showed good agreement to the dissolved fraction of the melt-milled SCS for the first five minutes. Subsequent deviations could be explained by primary particle agglomeration as well as the unpredictable fluid flow conditions in the USP apparatus II by excluding the influence of particle anisotropy and polymorph form.

Nevertheless, the phase-field approach can capture the physics of the dissolution process. This tool may be valuable to identify critical parameters for further improvements of the dissolution kinetics of low aqueous soluble drug substances and their formulation concepts.

Table
Glossary of symbols.

Symbol	description	SI-units
D	Diffusivity of drug substance in water	$m^2 \cdot s^{-1}$
$\bar{D}$	Phase averaged diffusivity	$m^2 \cdot s^{-1}$
d	Diameter	m
d_0	Initial diameter	m
$d_{2/1}$	Two dimensional Sauter diameter	m
d_{50}	Particle diameter at 50 % in the cumulative distribution	m
d_{90}	Particle diameter at 90 % in the cumulative distribution	m
k	Binary partition coefficient	–
k_{SR}	Surface reaction coefficient	$m^2 \cdot s^{-1}$
m_l	Slope of the liquidus line	K
m_R	Remaining particle mass	kg
m_0	Initial particle mass	kg
Re_m	Median particle Reynolds number	–
Sc	Schmidt number	–
Sh_m	Median Sherwood number	–
T	Temperature	K
T_m	Melting temperature	K
t	time	s
v_m	Median velocity	$m \cdot s^{-1}$
v_n	Normal interface velocity	$m \cdot s^{-1}$
w	Weight fraction	–
w_{solid}	Weight fraction of the solid	–
Γ	Gibbs-Thomson coefficient	m·K
δ_{SR}	Interfacial thickness	m
η	Dynamic viscosity	$kg \cdot m^{-1} \cdot s^{-1}$
μ_k	Linear kinetic coefficient	$K \cdot s \cdot m^{-1}$
ρ_{liquid}	Density of the liquid	$kg \cdot m^{-3}$
ρ_{solid}	Density of the solid	$kg \cdot m^{-3}$
σ	Surface tension	$kg \cdot s^{-2}$
σ'	Surface tension tensor	$kg \cdot s^{-2}$
Φ	Phase	–

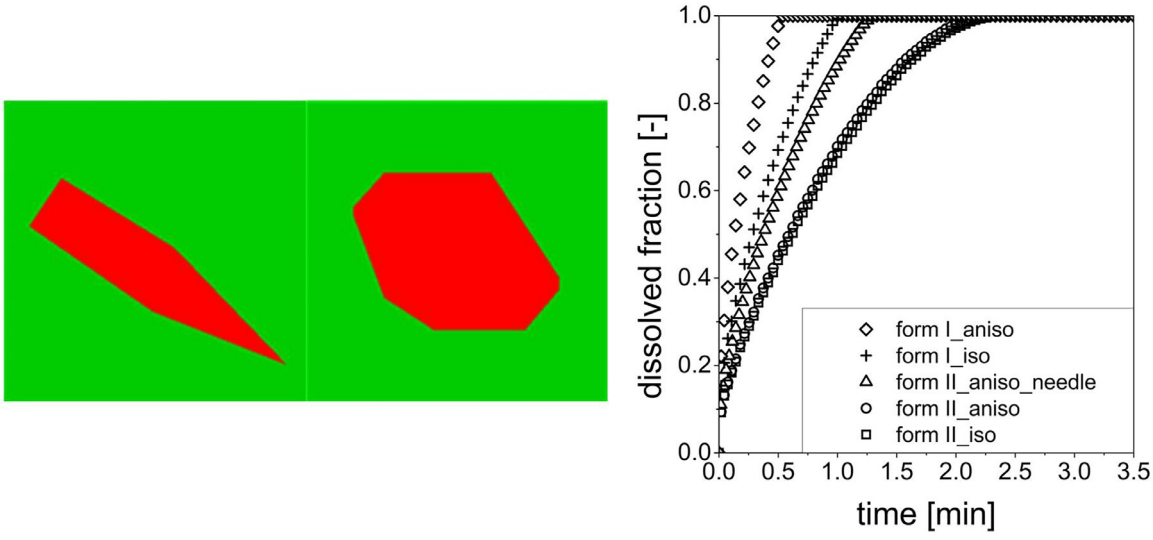

Fig. 8. Griseofulvin polymorphs form I and form II based on Su, et al.[55] (left). Dissolved fraction the anisotropic and isotropic polygons representing the griseofulvin morphologies form I and form II (right).

Declaration of competing interest

The authors declare that they have no known competing financial interests or personal relationships that could have appeared to influence the work reported in this paper.

Data Availability Statement

The data that support the findings of this study are available from the corresponding author upon reasonable request.

Acknowledgment

The authors are grateful for the support of Mr. Andrew Sittley for his MATLAB work and Ms. Meuris for the help in creating the SEM images.

References

1. Kawabata Y, Wada K, Nakatani M, et al. Formulation design for poorly water-soluble drugs based on biopharmaceutics classification system. Basic approaches and practical applications. *Int J Pharm*. 2011;420:1–10.
2. Amidon G, Lennernäs H, Shah V, Crison J. A theoretical basis for a biopharmaceutic drug classification. the correlation of in vitro drug product dissolution and in vivo bioavailability. *Pharm Res*. 1995;12:413–420.
3. Leane M, Pitt K, Reynolds GK, et al. Manufacturing classification system in the real world. factors influencing manufacturing process choices for filed commercial oral solid dosage formulations, case studies from industry and considerations for continuous processing. *Pharm Dev Technol*. 2018:1–59.
4. Fick A. Ueber Diffusion. *Ann Phys*. 1855;170:59–86.
5. Noyes AA, Whitney WR. The rate of solution of solid substances in their own solutions. *J Am Chem Soc*. 1897;19:930–934.
6. Hixson AW, Crowell JH. Dependence of reaction velocity upon surface and agitation. *Ind Eng Chem*. 1931;23:923–931.
7. Higuchi T. Rate of release of medicaments from ointment bases containing drugs in suspension. *J Pharm Sci*. 1961;50:874–875.
8. Ji Y, Paus R, Prudic A, et al. A novel approach for analyzing the dissolution mechanism of solid dispersions. *Pharm Res*. 2015;32:2559–2578.
9. Dokoumetzidis A, Papadopoulou V, Valsami G, Macheras P. Development of a reaction-limited model of dissolution. Application to official dissolution tests experiments. *Int J Pharm*. 2008;355:114–125.
10. Boettinger WJ, Warren JA, Beckermann C, Karma A. Phase-field simulation of solidification. *Annu Rev Mater Res*. 2002;32:163–194.
11. Saylor DM, Kim C-S, Patwardhan DV, Warren JA. Diffuse-interface theory for structure formation and release behavior in controlled drug release systems. *Acta Biomater*. 2007;3:851–864.
12. Li L, Zhu X, Yang H, et al. Phase-field model for drug release of water-swellable filaments for fused filament fabrication. *Mol. Pharm.*. 2022;19:2854–2867.
13. van den Mooter G. The use of amorphous solid dispersions. A formulation strategy to overcome poor solubility and dissolution rate. *Drug Discovery Today: Technol*. 2012;9:e79–e85.
14. Leuner C, Dressman J. Improving drug solubility for oral delivery using solid dispersions. *Eur J Pharmaceut Biopharmaceut*. 2000;50:47–60.
15. Thommes M, Ely DR, Carvajal MT, Pinal R. Improvement of the dissolution rate of poorly soluble drugs by solid crystal suspensions. *Mol. Pharm.*. 2011;8:727–735.
16. Nernst W. Theory of reaction velocity in heterogenous systems. *Zeit Physikal Chem*. 1904;47:52–55.
17. Brunner E. Reaktionsgeschwindigkeit in heterogenen Systemen. *Zeitschrift für Physikalische Chemie*. 1904;47:56–102.
18. Vasconcelos T, Sarmento B, Costa P. Solid dispersions as strategy to improve oral bioavailability of poor water soluble drugs. *Drug Discov Today*. 2007;12:1068–1075.
19. Muehlenfeld C, Kann B, Windbergs M, Thommes M. Solid dispersions prepared by continuous cogrinding in an air jet mill. *J Pharm Sci*. 2013;102:4132–4139.
20. Reitz E, Vervaet C, Neubert RHH, Thommes M. Solid crystal suspensions containing griseofulvin – preparation and bioavailability testing. *Eur J Pharmaceut Biopharmaceut*. 2013;83:193–202.
21. Ostwald W. Über die vermeintliche Isomerie des roten und gelben Quecksilberoxyds und die Oberflächenspannung fester Körper. *Zeitschrift für physikalische Chemie*. 1900;34:495–503.
22. Freundlich H, Hatfield HS. *Colloid and Capillary Chemistry*. London: Methuen And Co. Ltd; 1926.
23. Finke JH, Niemann S, Richter C, et al. Multiple orifices in customized microsystem high-pressure emulsification. The impact of design and counter pressure on homogenization efficiency. *Chem Eng J*. 2014;248:107–121.
24. Kamiya S, Kurita T, Miyagishima A, Arakawa M. Preparation of griseofulvin nanoparticle suspension by high-pressure homogenization and preservation of the suspension with saccharides and sugar alcohols. *Drug Dev Ind Pharm*. 2009;35:1022–1028.
25. Bitterlich A, Laabs C, Busmann E, et al. Challenges in nanogrinding of active pharmaceutical ingredients. *Chem Eng Technol*. 2014;37:840–846.
26. Loh ZH, Samanta AK, Sia Heng PW. Overview of milling techniques for improving the solubility of poorly water-soluble drugs. *Asian J Pharmaceut Sci*. 2015.
27. Beckermann C, Diepers H-J, Steinbach I, et al. Modeling melt convection in phase-field simulations of solidification. *J Comput Phys*. 1999;154:468–496.
28. Ely DR, Jana A, García RE. Phase field kinetics of lithium electrodeposits. *J Power Sources*. 2014;272:581–594.
29. Plapp M, Karma A. Eutectic colony formation: a phase-field study. *Phys Rev E Stat Nonlin Soft Matter Phys*. 2002;66:61608.
30. Boettinger WJ, Warren JA, Beckermann C, Karma A. Phase-field simulation of solidification. *Annu Rev Mater Res*. 2002;32:163–194.
31. Singer-Loginova I, Singer HM. The phase field technique for modeling multiphase materials. *Reports Progress Phys*. 2008;71: 106501.
32. Sleziona D, Ely DR, Thommes M. Modeling of particle dissolution behavior using a geometrical phase-field approach. *Mol. Pharm.*. 2022;19:3749–3756.
33. Guyer JE, Wheeler D, Warren JA. FiPy: partial differential equations with Python. *Comput Sci Eng*. 2009;11:6–15.
34. Owens DK, Wendt RC. Estimation of the surface free energy of polymers. *J Appl Polym Sci*. 1969;13:1741–1747.
35. Sjökvist E, Nyström C, Aldén M. Physicochemical aspects of drug release. XIII. The effect of sodium dodecyl sulphate additions on the structure and dissolution of a drug in solid dispersions. *Int J Pharm*. 1991;69:53–62.
36. Knoblauch J, Zimmermann I. Thermochemical analysis of the dissolution process of Griseofulvin. *Eur J Pharmaceut Biopharmaceut*. 2007;67:743–751.
37. Gombas A, Szabó-Révész P, Kata M, et al. Quantitative determination of crystallinity of α-lactose monohydrate by DSC. *J Therm Anal Calorim*. 2002;68:503–510.
38. Bringedal C, Wolff L von, Pop IS. Phase field modeling of precipitation and dissolution processes in porous media: upscaling and numerical experiments. *Multiscale Model Simul*. 2020;18:1076–1112.
39. Yang S, Ukrainczyk N, Caggiano A, Koenders E. Numerical phase-field model validation for dissolution of minerals. *Appl Sci*. 2021;11:2464.
40. Hester EW, Couston L-A, Favier B, et al. Improved phase-field models of melting and dissolution in multi-component flows. *Proc R Soc A*. 2020;476:20200508.
41. Kumar A, Prajapati N, Späth M, et al. Qualitative dissolution modeling of etch-pit formation on the K-feldspar surface through phase-field approach. *J Geophys Res: Solid Earth*. 2023;128: e2022JB025749.
42. Prajapati N, Späth M, Knecht L, et al. Quantitative phase-field modeling of faceted crystal dissolution processes. *Cryst Growth Des*. 2021;21:3266–3279.
43. Kukura J, Arratia PE, Szalai ES, Muzzio FJ. Engineering tools for understanding the hydrodynamics of dissolution tests. *Drug Develop Ind Pharmacy*. 2003;29:231–239.
44. McCarthy LG, Kosiol C, Healy AM, et al. Simulating the hydrodynamic conditions in the United States pharmacopeia paddle dissolution apparatus. *AAPS PharmSciTech*. 2003;4:E22.
45. Bai GE, Armenante PM, Plank RV, et al. Hydrodynamic investigation of USP dissolution test apparatus II. *J Pharm Sci*. 2007;96:2327–2349.
46. Bird RB, Stewart WE, Lightfoot EN. *Transport Phenomena*. New York: John Wiley & Sons; 1960:413.
47. Lochiel AC, Calderbank PH. Mass transfer in the continuous phase around axisymmetric bodies of revolution. *Chem Eng Sci*. 1964;19:471–484.
48. Balluffi RW, Allen S, Carter WC. *Kinetics of Materials*. John Wiley & Sons; 2005.
49. Ely DR, Edwin García R, Thommes M. Ostwald–Freundlich diffusion-limited dissolution kinetics of nanoparticles. *Powder Technol*. 2014;257:120–123.
50. Armenante P., Muzzio F. 2005. Inherent method variability in dissolution testing: the effect of hydrodynamics in the USP II apparatus.
51. Mugele RA, Evans HD. Droplet size distribution in sprays. *Ind Eng Chem*. 1951;43:1317–1324.
52. Wettlaufer JS, Jackson M, Elbaum M. A geometric model for anisotropic crystal growth. *J Phys A: Math Gen*. 1994;27:5957–5967.
53. Gao Z, Li C, Sun W, Hu Y. Anisotropic surface properties of calcite: a consideration of surface broken bonds. *Colloids Surf A: Physicochem Eng Aspects*. 2017;520:53–61.
54. Beckmann W. *Crystallization. Basic Concepts and Industrial Applications*. Weinheim: Wiley; 2013:362.. p.
55. Su Y, Xu J, Shi Q, et al. Polymorphism of griseofulvin: concomitant crystallization from the melt and a single crystal structure of a metastable polymorph with anomalously large thermal expansion. *Chem Commun*. 2018;54:358–361.
56. Mahieu A, Willart J, Dudognon E, et al. On the polymorphism of griseofulvin: identification of two additional polymorphs. *J Pharm Sci*. 2013;102:462–468.
57. Loginova I. *Phase-field Modeling of Diffusion Controlled Phase Transformations*. 28.10.2003. Stockholm, Sweden: KTH Royal Institute of Technology Stockholm Sweden. Department of Mechanics; 2003. PhD thesis.